Proceedings of SED2002
2002 International Solar Energy Conference
June 15-20, 2002, Reno, Nevada, USA

SED2002-1064

BEAM CHARACTERIZATION AND IMPROVEMENT WITH A FLUX MAPPING SYSTEM FOR DISH CONCENTRATORS

Steffen Ulmer, Wolfgang Reinalter, Peter Heller and Eckhard Lüpfert
Deutsches Zentrum für Luft- und Raumfahrt (DLR)
Plataforma Solar de Almería, Apartado 39
E-04200 Tabernas, Almería
Spain
e-mail: steffen.ulmer@psa.es
Phone: +34 950387935
Fax: +34 950365313

Diego Martinez
Centro de Investigaciones Energéticas
Medioambientales y Tecnológicas (CIEMAT)
Plataforma Solar de Almería, Apartado 22
E-04200 Tabernas, Almería
Spain

ABSTRACT

A flux mapping system able to measure the flux distribution of dish/Stirling systems in planes perpendicular to the optical axis was built and operated at the Plataforma Solar de Almería (PSA). It uses the indirect measuring method with a water-cooled Lambertian target placed in the beam path and a CCD-camera mounted on the concentrator taking images of the brightness distribution of the focal spot. The calibration is made by calculating the total power coming from the dish and relating it to the integrated gray value over the whole measurement area. The system was successfully operated in a DISTAL II stretched membrane dish and in the new EURODISH in order to characterize their beams and improve the flux distribution on their receivers.

INTRODUCTION

In the last 10 years, three generations of dish/Stirling systems (DISTAL I, DISTAL II and recently EURODISH) developed by Schlaich Bergermann und Partner (SBP) were tested and constantly improved at the Plataforma Solar de Almería (PSA). Good descriptions of these systems and their components have been given by Heller et al. [1, 2].

Flux measurements in the focal region of their concentrators play a key-role in optimizing the system efficiency. With a given receiver and cavity design the levers for optimizing the whole system are limited to the determination of the best receiver position and the most homogeneous flux distribution by modification of the tracking parameters and of the curvature of the reflective surface. Nevertheless, these measures can significantly increase the receiver input power and reduce the flux density peaks on the absorber and with them thermal stress and possible damage. Detailed measurements of the flux distribution in many planes from the focal region to the absorber plane of existing dishes are a valuable basis for future developments of system components like the optimization of the cavity design to further improve the receiver efficiency.

For that reason a flux-mapping device for dish/Stirling systems was built. In order to get the necessary high spatial resolution of the flux distribution, the indirect measurement method with Lambertian target and CCD-camera was chosen. Its measurement principle is the same as used in the system PROHERMES (programmable heliostat and receiver measurement system [3]) applied on the PSA for solar thermal power tower measurements.

EXPERIMENTAL SET-UP

The equipment consists basically of a target package with a water-cooled, moveable target plate placed in the beam path (Fig. 1 and Fig. 2), a CCD-camera fixed to the concentrator and a computer on the ground that controls target plate positioning and picture acquisition.

The used coordinate system has its origin in the intersection of the theoretical optical axis with the determined focal plane. Looking from the concentrator onto the target plate, the x-axis is the horizontal axis with positive values to the right and the y-axis is the vertical axis with positive values up. The z-axis is the optical axis with positive values away from the concentrator (Fig. 2).

Target package

The target plate of the package is made of a copper body with a milled cooling channel and sealed by a copper front plate. The front side is coated with plasma-sprayed Al_2O_3. Examination of the reflective properties was done with a Xenon ARC lamp with close to solar spectrum and a CCD-camera. At an observation angle of 0° (EURODISH setup) this coating has Lambertian properties within +5 % for incident angles close to the observation angle and –2 % for incident angles close to 45°. At an observation angle of 20° the coating exhibits the same behavior in respect to the observation angle. It does not exhibit a glancing angle but back reflection, that means that the radiation coming from close to the camera position may be overestimated by up to 5% compared to the average. Properties for an observation angle of 42° (DISTAL 2 setup) were not available but supposed to be similar. During operation the target plate is water-cooled with a closed cooling water circuit and is designed to resist flux densities of up to 20 MW/m^2. However, measurements showed that at flux density levels above 10 MW/m^2 there appear little gray dots on the white surface. To avoid this, the allowed maximum flux density was limited to 8 MW/m^2 for all tests after newly coating the target plate with highly pure Al_2O_3. Measurements of the focal plane were

performed with reduced irradiation levels in the late afternoon.

The target plate is fixed to a stiff aluminum frame on a linear drive that allows remote controlled target plate positioning within 350 mm along the z-axis. The frame also allows the target plate to be manually displaced up to ±50 mm in the x- and y-axes. The alignment of the target and the linear drive in respect to the dish is within 0.3° in all elevations. All components of the target package except the target plate are covered by a radiation protection made of ceramic fiber plates at the front side and stainless steel sheets on the sides.

Figure 1: The target package in operation in the EURODISH

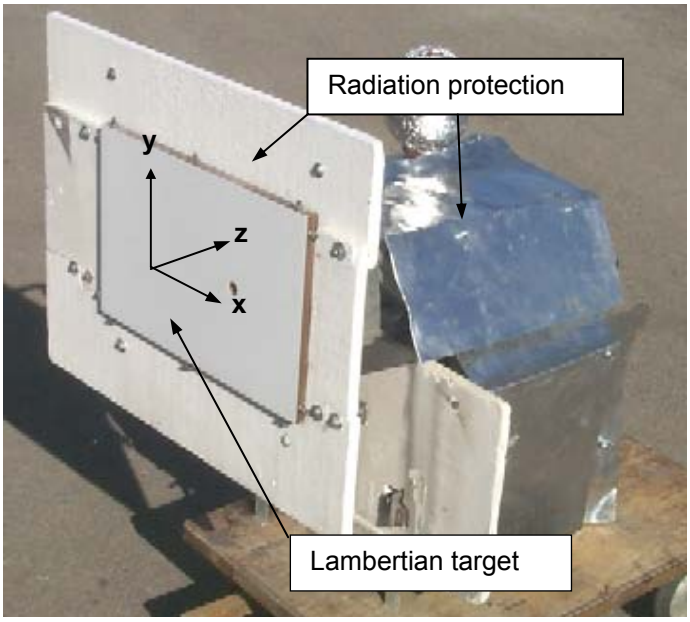

Figure 2: The target package on ground

CCD-camera system

The used camera is a THETA-SIS slow scan CCD-camera with a resolution of 286 x 384 pixels and 12-bit A/D converter. According to the manufacturer the linearity between brightness level and signal level is within 0.5 %. This accuracy could be confirmed by measuring the signal level of a constant light source (Ulbricht sphere) with different shutter times given by an electronic timer. The camera has a Peltier cooling to reduce and stabilize the dark current signal. It was set to 14.0 °C, the lowest possible temperature without condensation on the chip surface. The high brightness intensity of the focal spot is reduced with appropriate combinations of neutral density (ND-) filters. The camera with its controller was mounted in the DISTAL II system on a supporting beam at the side of the concentrator and in the EURODISH on a special camera support in the center of the concentrator.

Target control and image acquisition system

A PC in a container close to the dish equipped with the image processing software Optimas® remotely controls target plate positioning and image acquisition with a program written in the programming language ALI. The program communicates with the linear drive of the target package via serial port and moves the target plate in user-defined steps to the desired positions. Then the respective image is acquired and saved together with the information of the target plate position.

EVALUATION

Image correction

1. **Dark current**

Even without exposure to light CCD-chips give a dark current signal that depends on chip temperature and integration time. As the chip temperature is held constant, the dark current images can be acquired for each integration time used and later be subtracted from the measurement images.

2. **Shading**

Due to optical errors (shading) and tiny dust particles on the chip surface the camera and lens arrangement unequally rates the incoming light depending on the pixel position. This can be corrected with a correction matrix obtained from calculating the ratio for each pixel between the pixel gray value and the average gray value of an image of a uniformly bright surface achieved with an Ulbricht sphere.

3. **Rectification**

As the camera looks at the target at a certain angle and the relative size of the target plate varies with its z-position, the images need to be rectified and scaled. Two control pictures without ND-filters are taken, one in the home position of the linear drive and one in its end position. In a first step, the user marks the four corners of the target plate (points a-d, Fig. 3 left) and the software rectifies the images to the known target plate dimensions (Fig. 3 center). The error of the manual marking in an enlarged control picture is within ±0.5 pixel (±1 mm). In a second step, the left part of the target plate is cut out and saved in a standard format (Fig. 3 right). This procedure is repeated with all images taken during the measurements based on the control pictures. The corner positions of the target plate for linear drive positions between home position and end position are linearly interpolated. All images are filtered with a median-3*3 filter to reduce noise.

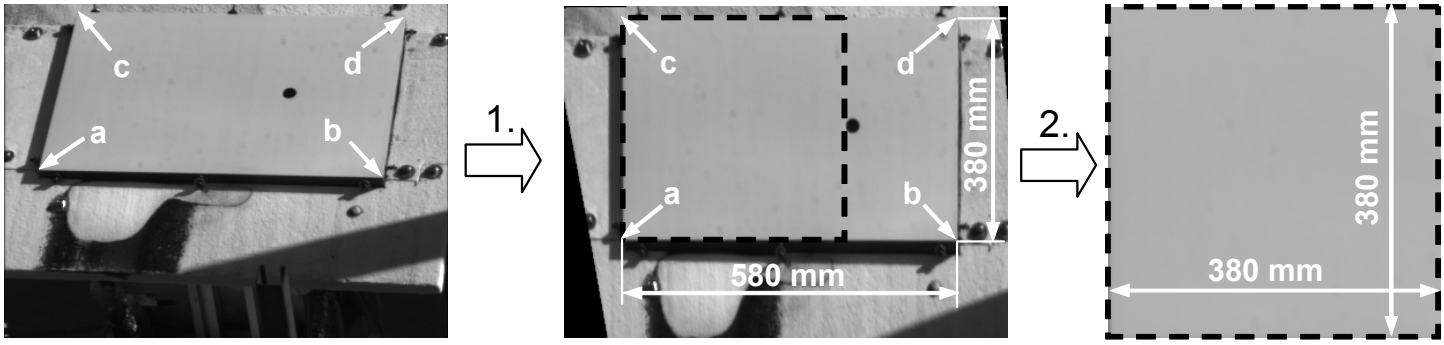

Figure 3: Image rectification and size standardization of used target area

Flux Density Calibration

Due to the Lambertian target properties, the brightness distribution on the target surface observed from any angle is linear to the flux density distribution on the target surface and independent on its incident angle. After image correction the gray value signal of the CCD-camera is linear to the brightness on the target surface. Hence, the gray values are linearly dependent on the incident flux density on the target (Eq. (1)).

$$E = F_c \cdot GV \tag{1}$$

With E = *Flux density*
F_c = *Calibration factor*
GV = *Gray value*

The factor F_c is usually obtained by measuring the irradiance at one point with a radiometer and comparing its reading with the gray value at the same position after moving in the target. However, available radiometers for the prevailing flux densities are not satisfactorily accurate [4] and the flux distribution in the focal plane exhibits very steep gradients that lead to large differences in flux density with little error in exact location. Hence, this type of calibration tends to be erroneous. Therefore, a different calibration procedure without radiometer has been used.

The calibration factor can be defined by the ratio of the total power on the target plate to the sum of gray values times the pixel area over the whole target surface:

$$F_c = \frac{P_{target}}{\sum_{i=1}^{Pixel} A_i \cdot GV_i} = \frac{P_{conc} \cdot \gamma_{target}}{\sum_{i=1}^{Pixel} A_i \cdot GV_i} = \frac{DNI \cdot \rho_{conc} \cdot (A_{conc} - A_{shadow} - A_{gap}) \cdot \gamma_{target}}{A_{target} \cdot GV_{mean}} \tag{2}$$

With A_i: = *Area of pixel I*
A_{conc} = *Effective surface of concentrator*
A_{gap} = *Lost area due to gaps between mirrors*
A_{shadow} = *Lost area due to shading*
A_{target} = *Target area*
DNI = *Direct Normal Irradiation*
GV_i = *Gray value of pixel i*
GV_{mean} = *Mean gray value on target area*
P_{conc} = *Total power from concentrator*
P_{target} = *Total power on target surface*
$Pixel$ = *Number of pixels in target area*
γ_{target} = *Target intercept factor*
ρ_{conc} = *Measured concentrator reflectivity*

The calibration is based on the calculation of the total power delivered by the concentrator and on the assumption that all this radiation hits the used target surface when the target plate is placed in or close to the focal plane where the focal spot is comparatively small. Calculations in the simulation code CIRCE [5] demonstrate that the power not intercepted by a circular target of 35 cm diameter in the focal plane lies in the range of 0.15 % to 1.4 % for sunshapes with circumsolar ratios of 5 % to 35 %, respectively. That means that the additional systematic error that this assumption introduces to the calibration error may be up to +1.4 % for extremely bad sunshapes. The uncertainty in the marking of the target area in the pictures is the side lengths ±1 pixel, which results in a maximum error in the area size of ±0.9 %.

The target intercept factor γ_{target} describes the ratio of the flux on the used target area to total flux coming from the concentrator. With increasing distance from the focal plane the size of the focal spot grows and not all of its energy hits the used target area: the target intercept factor decreases (see Fig. 6). However, γ_{target} can be calculated from the measurements by relating the integrated gray values of the used target area in the respective positions to the integrated gray values of the used target area in the focal plane when all values are taken in a short interval of time and are scaled with the respective direct normal irradiation. The DNI is measured with a tracked Eppley radiometer.

The calibration factor is constant if the relation between flux density and camera signal remains constant. Factors that change this relation are lens aperture, camera integration time, filter transmission and spectral CCD response. Aperture and filters are not changed during the measurements. However, the neutral density filters and the response of the camera are not flat over the whole spectral range of sunlight. The transmission of the ND-filters in the infrared range is by far higher than their design transmission in the visible range (Fig. 4). It also shows that the camera response has its peak in the range of 750 nm and is sensitive in the infrared up to 1,100 nm. As the spectral

composition of sunlight changes throughout the day with changing air mass (AM, factor that describes the multiple of the pathlength of the solar radiation through the atmosphere in reference to the shortest possible path when sun is in zenith) and atmospheric conditions, the effective transmission of the ND-filters and the sensitivity of the camera also change. Figure 5 shows the calculated effect on the calibration factor by changing air mass with spectral data taken from MODTRAN 3.5 simulations based on the ASTM standard data set for 1.5 AM. The solar spectrum shifts to the infrared at high air masses and due to the higher transmission of the ND-filters at these wavelengths this leads to an overestimation of more than 20 % for AM5 compared to AM1 for a constant calibration factor. Similar calculations on the spectral influence on CCD-camera measurements were reported by Kaluza [6]. However, correction of this error is difficult because it does not only depend on the air mass at the measurement but also on the prevailing atmospheric conditions which are not exactly known. Therefore, it was not possible to use a constant calibration factor for all measurements with specific camera settings but to avoid this error the calibration factor for each measurement was calculated separately with Eq. (2). As the spectral composition of sunlight changes steadily, any calibration factors that could not be determined with the equation were linearly interpolated. Measurements in different planes for the determination of target intercept factors beyond the focal region were made in a short interval of time to keep the spectral influence small.

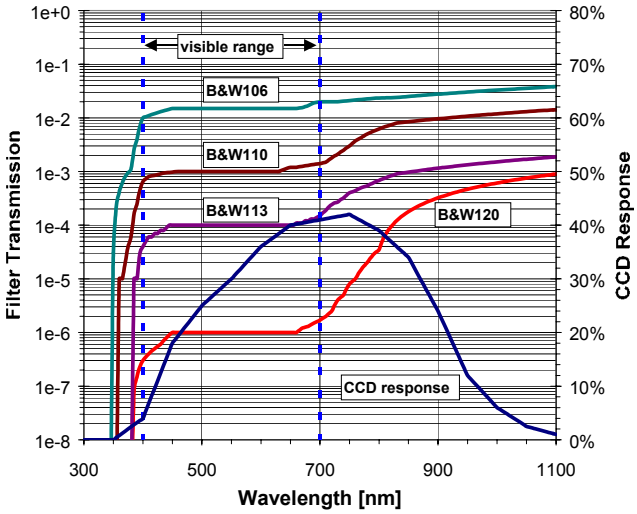

Figure 4: Transmission curves of B&W ND-filters

Normalization

In order to get comparable test results that are independent of the prevailing solar irradiation and concentrator condition, the measurements are normalized to the following set of standard conditions. The used standard irradiation is 1,000 W/m^2 and standard mirror reflectivity of a clean concentrator is ρ_{conc}= 0.94. These values with the respective concentrator geometries and shading losses that were determined with digital image analysis with an error within ±0.25 m^2 (±0.5 %) give a standard total concentrator power of 49.39±0.25 kW for the DISTAL II dishes and 49.91±0.25 kW for the EURODISH. All flux density results presented in this paper refer to normalized values and equal concentration factors expressed in suns.

Error calculation

Table 1 gives an overview of the error sources mentioned in the previous paragraphs and an estimation of the maximum total error of the measurements. Some errors (noise etc.) have no influence on the calibration because they equal out over the whole target area but they do have an effect on the values of single pixels, therefore the error is divided in the calibration error and the maximum error of a single pixel. The uncertainty of the direct normal irradiation measurements and the mirror reflectivity measurements do not enter in the total error because the measurements are all normalized to standard conditions.

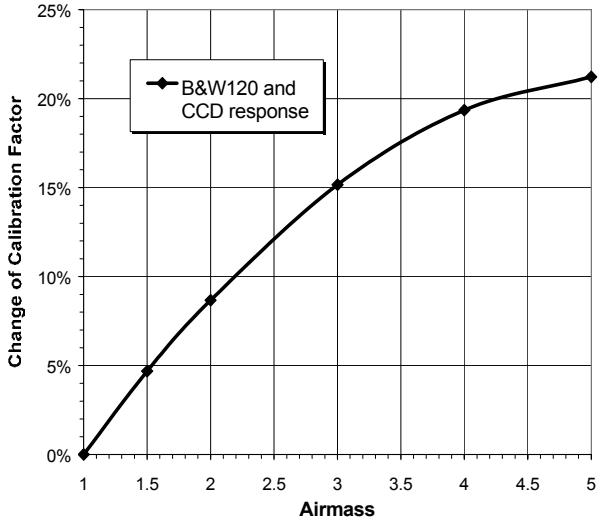

Figure 5: Spectral influence on calibration factor

Table 1: Error sources and total error of measurements

Error source	Calibration error	Error of single pixel
Camera/Optics:		
Linearity	±0.5%	±0.5%
Noise (darkcurrent, photon, readout)		±0.5%
Spectral error	±0.25%	±0.25%
Target:		
Lambertian properties		-2% / +5%
Alignment (within 0.3°)		±1.25%
Calibration/Evaluation:		
Target intercept	0% / +1.4%	0% / +1.4%
Mean GV based on marked rectangle	±0.9%	±0.9%
Effective concentrator area	±0.5%	±0.5%
Interpolation of missing calibration factors	±0.25%	±0.25%
Maximum total error	**-2.4% / +3.8%**	**-6.15% / +10.55%**

These errors are maximum absolute errors of the measurements. In many cases, however, relative changes in the flux distribution are measured and in these comparisons the error is much lower.

RESULTS

The measurement system was employed at PSA in January 2001 in the stretched-membrane dish DISTAL II North and in July 2001 in the EURODISH South. Measurements in planes behind the aperture plane (positive z-values) do not consider the influence of the blocking of the aperture plate and the reflection from the cavity walls on the flux distribution. Any effects of different sunshapes due to changes in atmospheric conditions on the flux distributions are not considered.

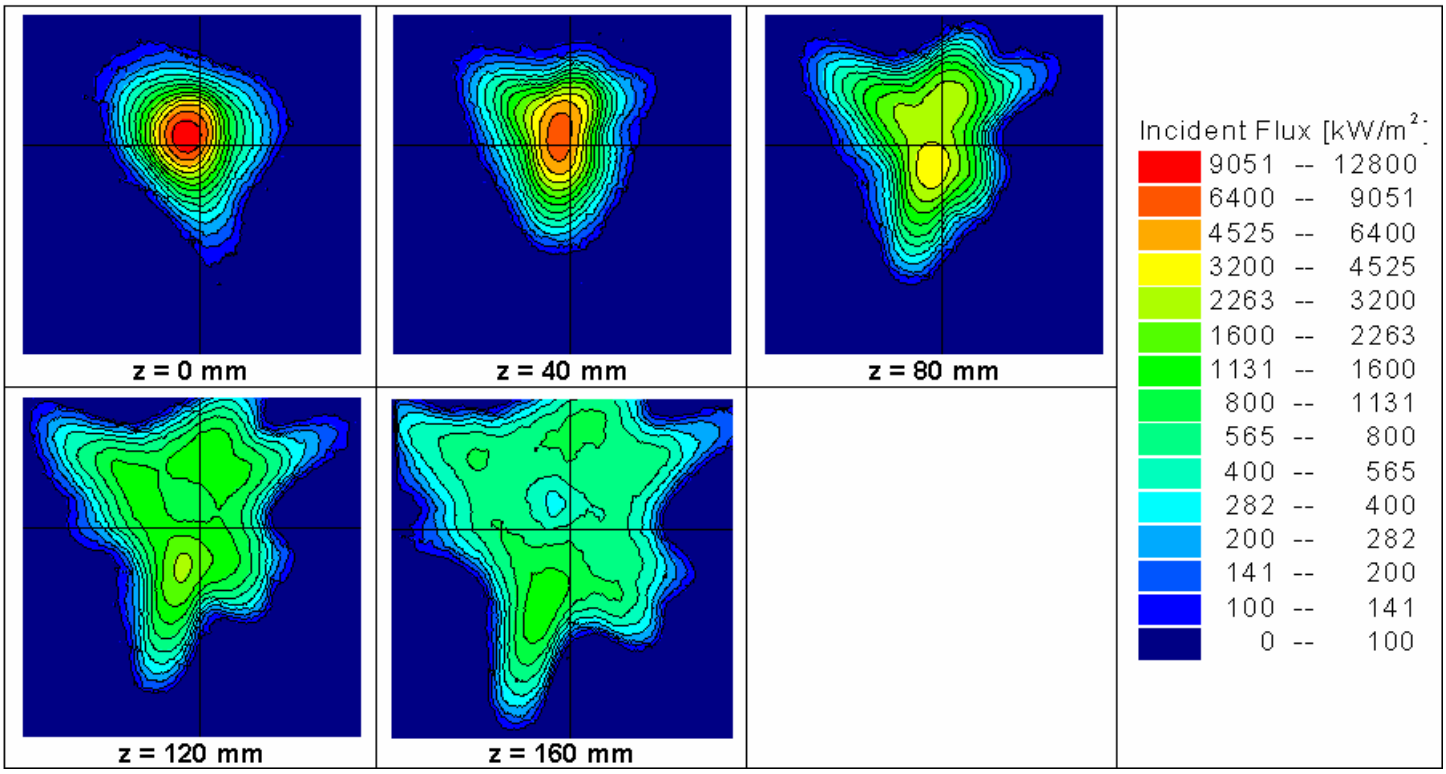

Figure 6: Flux maps from focal plane to absorber plane in logarithmic scale

DISTAL II North

DISTAL II North is a stretched-membrane dish with a diameter of 8.5 m and a focal length of 4.98 m. Figure 6 shows the characterization of the focal spot from the focal plane (z = 0 mm) to the absorber plane (z = 160 mm) in 40 mm steps. The color levels are logarithmically scaled in order to visualize the large differences in flux density using the same scale. It can be seen that almost all the energy coming from the concentrator hits the target surface in the planes close to the focal plane. In planes further off the focal plane the spot size increases and some energy misses the used target area. Leaving the focal plane the nearly symmetrical shape becomes more and more an irregular, star-like shape with an inhomogeneous flux distribution.

Figure 7 shows the normalized flux distribution in the focal plane in detail. The axis crossing shows the position of the theoretical optical axis of the concentrator. The focus shape is a slightly oval Gaussian distribution with a peak flux of 11,960 kW/m^2 and a 90 % radius of 96 mm. The center is at x_{center} = -20 mm to the left and y_{center} = +9 mm above its theoretical position. The intercept factor for the DISTAL II aperture with a radius of 90 mm around the weighted center of the focal spot (circle) in this plane is 88.5 %. The real aperture intercept with its center in the theoretical optical axis is 87.4 % which means that the incoming power could be increased by 1.2 % by relocating the package or by changing the tracking offset by x = +20 mm and y = -9 mm.

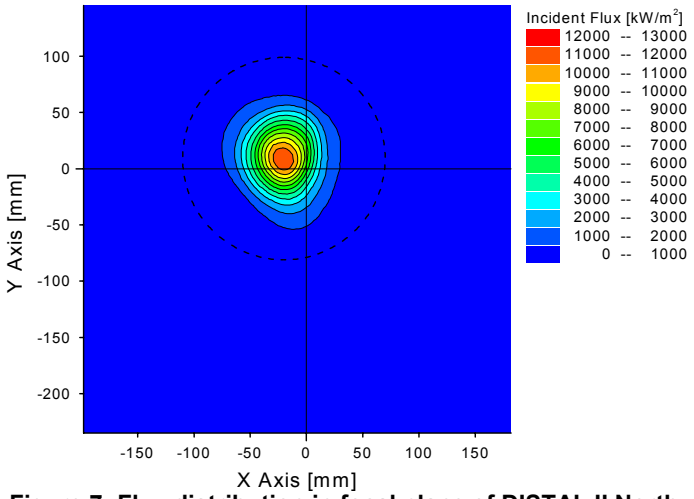

Figure 7: Flux distribution in focal plane of DISTAL II North

The receiver has a hexagonal shape with an inscribed circle of 130 mm radius and is located 160 mm behind the focal plane. This plane is shown in Fig. 8. It can be seen that the distribution has an irregular shape with a pronounced flux density peak of 1,520 kW/m^2 in the lower left part whereas other parts of the receiver area (hexagon) receive much lower flux densities. The mean flux density on the receiver area is 611 kW/m^2 with a peak to mean flux density ratio of 2.48. The weighted center of the focal spot is located to the left at x_{center} = -21 mm and y_{center} = +4 mm. The receiver intercept factor is 72.5 %.

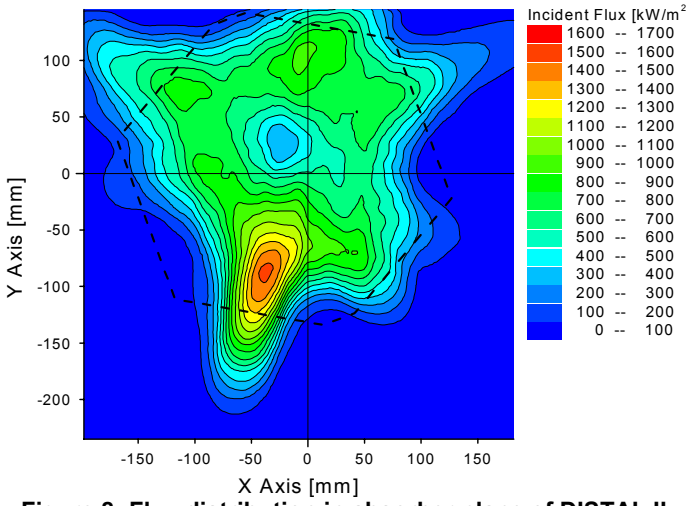

Figure 8: Flux distribution in absorber plane of DISTAL II North

The flux distribution in the absorber plane can be slightly varied by applying an offset to the sun-tracking algorithm of the concentrator. This was done in order to reduce the detected flux density peak and to obtain a more homogeneous flux distribution on the receiver area. The tracking offset of the concentrator was changed in a grid of 9 mm steps around the default. The most homogeneous distribution with the lowest peak flux value was found at an offset position of 36 mm to the left and 36 mm downward (Fig. 9). The weighted center of the focal spot moved to x_{center} = -56 mm and y_{center} = -31 mm. The flux distribution shifted partly from the lower left to the upper right side. As a result, the flux density peak could be reduced by about 23.6 % to 1,230 kW/m^2 and the receiver intercept factor increased to 74.4 %. The mean flux density on the receiver area is now 627 kW/m^2, which results in a peak to mean flux density ratio of 1.96. Relocating the power package to this position and operating the dish with the found tracking offset would allow to run the receiver with 2.6 % more direct radiation and much lower peak flux density levels. This would significantly reduce the material stress of the absorber tubes.

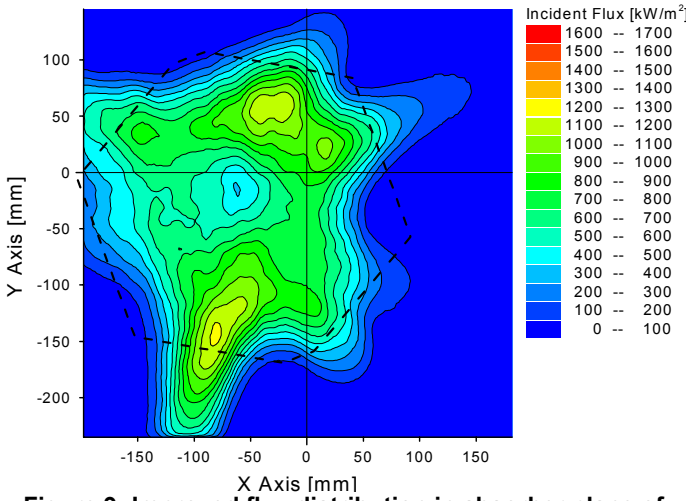

Figure 9: Improved flux distribution in absorber plane of DISTAL II North

The receiver input power and with it the system efficiency could be further increased if the power package was positioned closer to the focal plane after reducing the flux density peaks. Figure 10 shows the development of peak flux densities and of receiver intercept factors over the distance from focal plane to absorber plane extracted from the series in Fig. 6. It can be seen that about 15 mm closer to the focal plane, at z ≈ 145 mm, the maximum flux levels with the found tracking offset are the same as at z = 160 mm without offset (arrow 1). Yet, at this distance (arrow 2) the receiver intercept factor is about 79.5 % (arrow 3). This means that the radiation that directly hits the receiver could be increased in total by 9.6 % with the same peak flux density on the absorber as up to now but with a more uniform flux distribution.

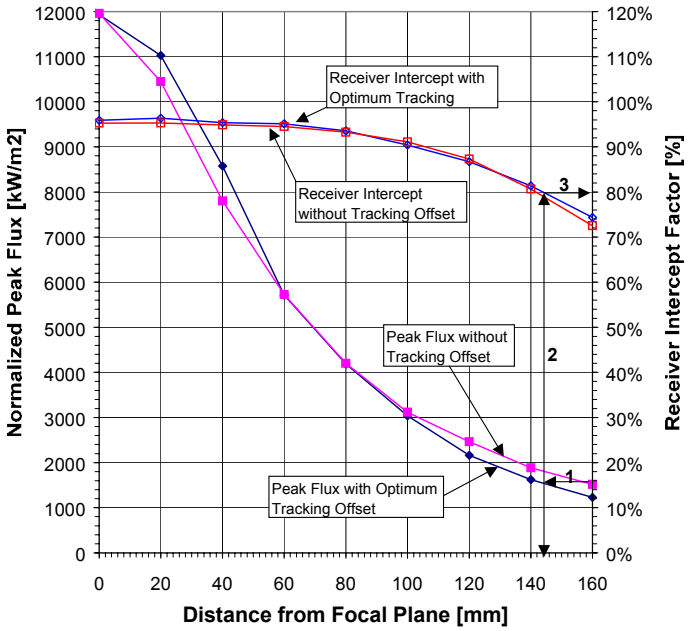

Figure 10: Possible improvement of receiver intercept factor with tracking offset

Variations of the partial vacuum between the stretched membranes within the allowed limits from 20 mbar to 35 mbar only changed the focal length about 10 mm but had no effect on the flux distribution in the absorber plane.

EURODISH South

The EURODISH has a concentrator shell of 8.5 m diameter and a focal length of 4.5 m. As it is a newly built system the flux measurement system could be used directly in the setup process to optimize the position of the power package. Figure 11 shows the normalized flux density distribution in the focal plane. The theoretical optical axis of the concentrator (axis crossing) is in the center of the target. The focus shape is close to a symmetric Gaussian distribution with a peak flux of 12,730 kW/m2 and a 90 % radius of 72 mm. The center is at x_{center} = -1 mm to the left and y_{center} = -7 mm below its theoretical position. The intercept factor for the larger EURODISH aperture with a radius of 120 mm around the weighted center of the focal spot in this plane is 98.0 %. The real aperture intercept with its center in the theoretical optical axis is 97.6 %, which means that the incoming power is close to the optimum value. It could be increased

only 0.4 % by relocating the package or by changing the tracking offset to its optimum.

Compared to the DISTAL II North it can be seen that the focal spot is more symmetric and the maximum flux density is about 790 kW/m^2 higher. The 90 % radius is with 72 mm significantly smaller than the 96 mm measured at the stretched membrane dish.

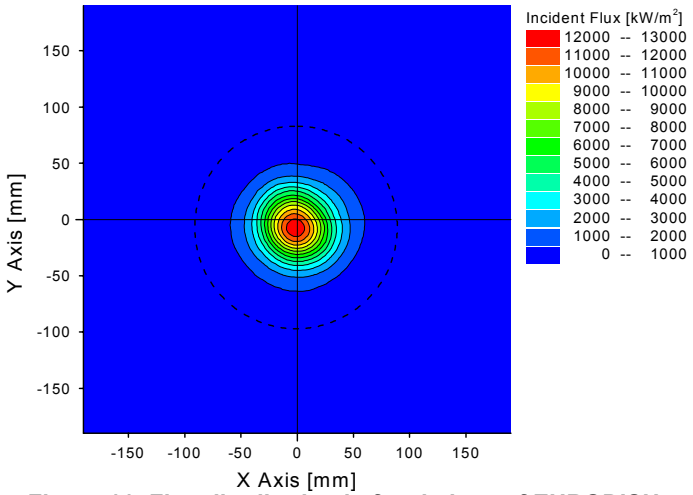

Figure 11: Flux distribution in focal plane of EURODISH South

In the absorber plane in Fig. 12 it can be seen that the flux distribution has a much more symmetric shape but has a pronounced flux density peak of 1,640 kW/m^2 in the center. The mean flux density on the receiver area is 686 kW/m^2 with a peak to mean flux density ratio of 2.39. The weighted center of the focal spot is located to the left at x_{center} = -2 mm and below at y_{center} = -5 mm and the receiver intercept factor is 80.5 %.

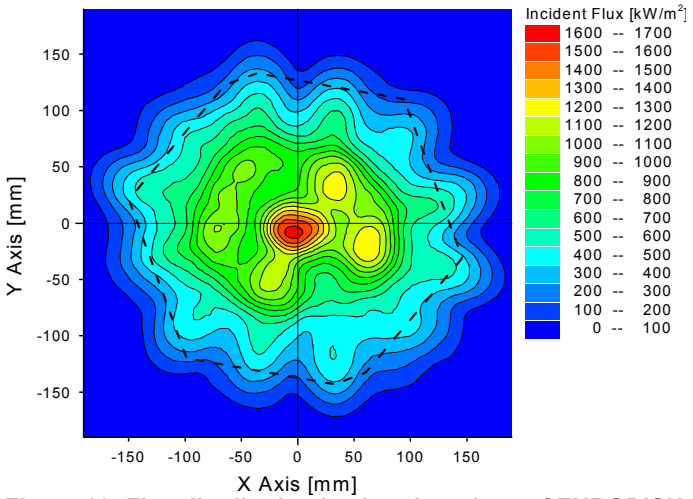

Figure 12: Flux distribution in absorber plane of EURODISH South

The high flux density peak in the center resulted from a slightly changed facet curvature in the inner part of the concentrator shell during the manufacturing process. This was corrected during the put-into-operation of the prototype and led to the desired optical quality. The initial concentrator curvature caused the focal length of the inner part of the concentrator to be too long and to focus behind the desired focal plane. This was the reason for the high flux density peak in the center of the absorber. By applying tension forces from the center ring of the concentrator to the support structure behind, this effect could be greatly reduced. The tension was gradually increased and flux measurements were made until the optimum flux distribution was found. The flux density peak could be reduced by 20.6 % to 1,360 kW/m^2 and the receiver intercept factor slightly increased to 80.9 % (Fig. 13). The mean flux density on the receiver area is now 690 kW/m^2, which results in a peak to mean flux density ratio of 1.97.

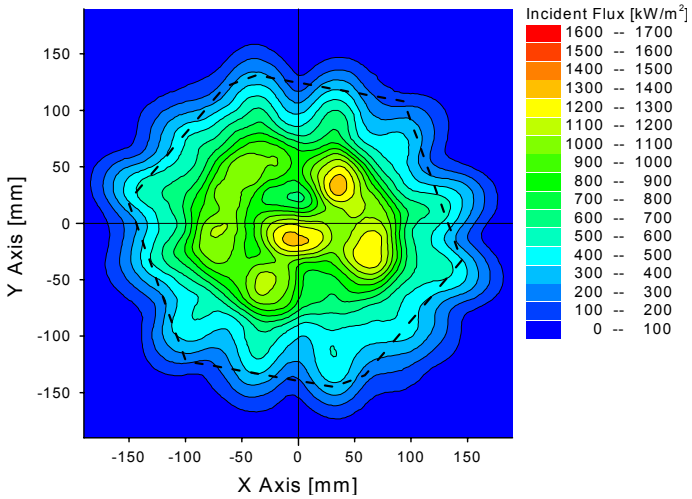

Figure 13: Improved flux distribution after applying tension ring on concentrator center

The tracking offset of the concentrator was changed in a grid of 15 mm steps around the default in order to find the best tracking offset. However, as the flux distribution in the default position is already close to symmetric, the distribution could only be improved slightly. The best position was found at 15 mm up with a peak flux density of 1,300 kW/m^2 and the same receiver intercept factor. This would make the center move up about 15 mm and so locate it 7 mm above the theoretical optical axis.

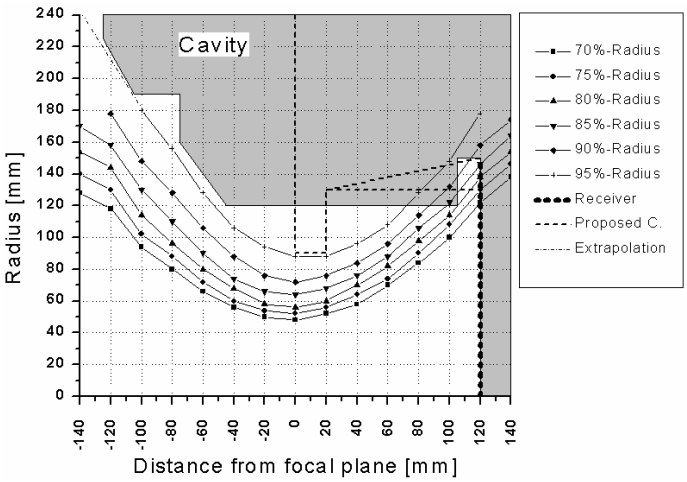

Figure 14: Percentage of integrated energy radii and cavity outline in EURODISH South

Figure 14 displays the cavity outline and the measured integrated energy radii in the EURODISH South. Radii of more than 180 mm are extrapolated with a polynomial data fit because they are beyond the target limits. It can be seen that the restraining element is not the aperture opening in the focal plane but the ceramic radiation protection with a radius of 220 mm about 120 mm in front of it. About 95 % of the total reflected energy pass this plane and enter the cavity, 15 % hit the cavity walls in the very rear part and the remaining 80 % pass through the rear cavity opening with a radius of 120 mm. It can be seen that the circular cavity opening is not ideal for the hexagonal receiver, as the corners (radius = 150 mm) are not irradiated and some of the radiation will miss the receiver where its radius is small (130 mm). The aperture opening with a radius of 120 mm in the focal plane would theoretically let pass 98 % of the total energy and so it is needlessly big because only 95 % pass the radiation protection. Its radius could be reduced to 90 mm without blocking any more incoming radiation and consequently reduce reflection, radiation and convective losses from within the cavity. The dashed line in Fig. 14 shows a proposed cavity outline with hexagonal rear opening for future improvements based on the measured data. The blocking caused by the ceramic protection in front of the focal plane could also be avoided with this geometry. However, this graphical analysis gives just an idea of the possible improvements. Calculations need to be done to find the best cavity design and determine the possible gains in efficiency.

SUMMARY

The described system allows the measurement of the flux distribution of dish/Stirling systems in any plane perpendicular to the optical axis. The indirect measuring method with the described calibration method maps the flux distribution with high spatial resolution and good accuracy without using a radiometer. The error of the calibration method was determined to be within –2.4 % and +3.8 % while single pixels have a maximum absolute error of –6.15 % to +10.55 %. After initial tests with the target plate coating the flux density was limited to 8 MW/m^2 to avoid damage.

The focal plane of the dish DISTAL II North was determined and measurements between this plane and the absorber plane were performed. The maximum concentration in the focal plane was found to be 11,960 kW/m^2 with a 90 % radius of 96 mm. The flux distribution in the absorber plane was found to be inhomogeneous with areas of high flux densities. Giving an offset to the sun-tracking algorithm could moderate this unevenness. The peak flux density on the absorber could be reduced by more than 20 % from 1,520 kW/m^2 to 1,230 kW/m^2 and the receiver intercept factor could be slightly increased to 75.4 %. The more homogeneous flux distribution would allow moving the receiver 15 mm closer to the focal plane without stressing the receiver more than up to now. This would further increase the receiver intercept factor to 79.5 %.

The measurement system was also used to optimally setup the EURODISH South. It was found that the dish concentrates slightly higher in the focal plane (12,730 kW/m^2) and has a significantly smaller 90 % radius of 72 mm. The flux distribution in the absorber plane is much more symmetrical. The peak flux density in the absorber plane could be reduced by about 20 % from 1,640 kW/m^2 to 1,360 kW/m^2 by applying a tension ring to the center of the concentrator and additional 4.6 % to 1,300 kW/m^2 by changing the tracking offset. The receiver intercept factor increased slightly from 80.5 % to 80.9 % and is about 5 % higher than the intercept factor of the DISTAL II dish. Measurements in planes up to 140 mm in front and behind the focal plane revealed that the design of the cavity and of the radiation protection could be improved and an optimized design based on the data is proposed.

ACKNOWLEDGEMENTS

Thanks to M. Homburg, M. Laps and T. Rauch for their important contributions within their scholarships and to A. Neumann for the sunshape data, spectral data and the design of the target plate. Thanks also to Guillermo Velasco and other involved PSA and DLR colleagues for their support during construction and operation of the flux mapping system.

REFERENCES

[1] Heller, P.; Reinalter, W., Martínez, D., 2001, “Status of Development of the Dish/Stirling Systems at Plataforma Solar de Almería”, Proceedings of 10th International Stirling Engine Conference 2001, Osnabrück, Germany.

[2] Heller, P., Baumüller, A., and Schiel, W., 2000, “Eurodish – The Next Milestone to Decrease the Costs of Dish/Stirling Systems Towards Competitiveness”, Solar Thermal 2000 International Conference”, Sydney, Australia

[3] Lüpfert, E., Heller, P., Ulmer, S., Monterreal, R., and Fernández, J., 2000, “Concentrated Solar Radiation Measurement with Video Image Processing and Online Fluxgage Calibration”, Solar Thermal 2000 International Conference”, Sydney, Australia

[4] Kaluza, J., Neumann, A., Ferriere, A., Robert, J.F., 2000, “Concentrated Solar Flux Measurements: Results of the Second SolarPACES Fluxmeter Intercomparison Campaign”, 10th SolarPACES International Symposium on Solar Thermal Concentrating Technologies, Sydney, Australia

[5] Romero, V. J., 1994, “CIRCE2/DEKGEN2: A Software Package for Facilitated Optical Analysis of 3-D Distributed Solar Energy Concentrators”, User Manual, Sandia Report SAND91-2238, Albuquerque, New Mexico

[6] Kaluza, J., Neumann, A., 1998, “Measurement of Solar Radiation with CCD-Cameras: Influence of the Spectral Characteristic”, ASME/Solar '98, Albuquerque, ASME